FEBS Letters 589 (2015) 3271–3276

FEBS Letters

journal homepage: www.FEBSLetters.org

Dissecting the functional roles of the conserved NXXE and HXE motifs of the ADP-dependent glucokinase from *Thermococcus litoralis*

María José Abarca-Lagunas, Jaime Andrés Rivas-Pardo [1], César A. Ramírez-Sarmiento *, Victoria Guixé *

Departamento de Biología, Facultad de Ciencias, Universidad de Chile, Las Palmeras 3425, Casilla 653, Santiago 7800003, Chile

ARTICLE INFO

Article history:
Received 21 August 2015
Revised 11 September 2015
Accepted 20 September 2015
Available online 30 September 2015

Edited by Miguel De la Rosa

Keywords:
Archaeal enzyme
Glucokinase
ADP-dependent kinase
Protein–ligand binding
Divalent metal cation

ABSTRACT

The activity of the ADP-dependent glucokinase from *Thermococcus litoralis* (*Tl*GK) relies on the highly conserved motifs NXXE (i.e. Asn-Xaa-Xaa-Glu) and HXE (i.e. His-Xaa-Glu). Site-directed mutagenesis of residues Glu279 (HXE) and Glu308 (NXXE) leads to enzymes with highly reduced catalytic rates. The replacement of Glu308 by Gln increased the K_M for $MgADP^-$ and was activated by free Mg^{2+}. On the other hand, HXE mutants did not affect the K_M for $MgADP^-$, were still inhibited by free Mg^{2+}, and caused a large increase on K_M for glucose and an 87-fold weaker binding of glucose onto the non-hydrolysable *Tl*GK·AMP–AlF_3 complex. Our findings put forward the fundamental role of the HXE motif in glucose binding during ternary complex formation.

1. Introduction

Glucose phosphorylation into glucose-6-phosphate (glucose-6-P) constitutes the first step of glycolysis, the central metabolic pathway in all three domains of life. While most glucokinases use adenosine triphosphate (ATP) as the phosphoryl donor, several archaea of the *Euryarchaeota* possess an ADP-dependent glucokinase as part of a variety of modifications on their Embden–Meyerhof pathway [1]. Despite the lack of sequence similarity between these glucokinases and their ATP-dependent counterparts, the three-dimensional structure resolution of several of these ADP-dependent enzymes have allowed their classification as members of the ribokinase superfamily [2]. Structurally, these archaeal glucokinases are composed by two domains: a large α/β/α domain whose topology corresponds to a Rossmann-like fold [2,3] that constitutes the core structure for all members of the ribokinase superfamily [4]; and a small domain composed of a five-stranded β-sheet, which is embellished with several α-helices that are commonly present in monomeric members of this superfamily [5]. These domains are connected by four chain crossings due to an intertwined polypeptide topology, which has been shown to promote cooperativity across these domains in other members of the ribokinase superfamily [6].

Among the structures of ADP-dependent glucokinases that have been solved to date, belonging to the archaeal species *Thermococcus litoralis* [2,7], *Pyrococcus horikoshii* [8] and *Pyrococcus furiosus* [9], the enzyme from *T. litoralis* (*Tl*GK) corresponds to the best characterized model in terms of its structure, function and kinetic mechanism. Thorough initial velocity analysis of the phosphotransferase reaction catalyzed by *Tl*GK using variable concentrations of substrates, products and inhibitors allowed determination of its kinetic mechanism, corresponding to a sequential ordered Bi–Bi model where the metal–nucleotide complex is the first substrate to bind to the enzyme, while glucose binds only when the *Tl*GK·$MgADP^-$ complex is already formed [7]. In line with this kinetic mechanism, small angle X-ray scattering and structure solution of *Tl*GK in the presence of substrates and analogs have shown that the large and small domains of *Tl*GK experience a sequential open-to-closed conformational transition, where $MgADP^-$ binding elicits a semi-closed state and the subsequent binding of glucose leads to formation of the ternary complex,

Abbreviations: ADP, adenosine-diphosphate; ATP, adenosine triphosphate; GK, glucokinase; *Tl*GK, glucokinase from *Thermococcus litoralis*; glucose-6-P, glucose-6-phosphate; K_M, Michaelis constant; k_{cat}, turnover rate; K_i, inhibition constant; K_a, activation constant; K_D, dissociation constant

Author contributions: C.A.R.S. and V.G. conceived and supervised the study; M.J.A.L., J.A.R.P., C.A.R.S. and V.G. designed experiments; J.A.R.P., M.J.A.L. and C.A.R.S. performed experiments; J.A.R.P., M.J.A.L. and C.A.R.S. analyzed data; M.J.A.L., J.A.R.P., C.A.R.S. and V.G. wrote the manuscript.

* Corresponding authors.

E-mail addresses: ceramirez@uchile.cl (C.A. Ramírez-Sarmiento), vguixe@uchile.cl (V. Guixé).

[1] Current address: Department of Biological Sciences, Columbia University, Northwest Corner Building, 550 West 120 Street, New York, New York 10027, United States.

http://dx.doi.org/10.1016/j.febslet.2015.09.013
0014-5793/

triggering total domain closure [7]. Moreover, this sequential binding of substrates in *Tl*GK has been recently confirmed by single-molecule force spectroscopy experiments [10].

Although *Tl*GK can exert its activity with similar catalytic efficiencies using Mg^{2+}, Mn^{2+} or Co^{2+} as part of the metal–nucleotide complex that constitutes its true phosphoryl donor substrate, it is also inhibited by increasing concentrations of free divalent cations in the low millimolar range [11]. The need of a second divalent cation for the regulation of the activity of these enzymes has been largely stressed by its direct structural observation and by assessment of its functional impact in other enzymes of the ribokinase superfamily, such as human adenosine kinase [5,12], human pyridoxal kinase [13,14], *Escherichia coli* phosphofructokinase-2 [15–17] and others [18,19].

Even when the catalytic consequences of increasing the concentration of free divalent cations can vary between different enzymes, in some cases leading to activation instead of inhibition [17,20], it has been widely demonstrated that the glutamate of a highly conserved motif for all members of the ribokinase superfamily, known as NXXE (i.e. Asn-Xaa-Xaa-Glu, Fig. 1), is responsible of the catalytic and regulatory effect elicited by divalent metals in these enzymes [15,20]. However, recent sequence analysis and molecular dynamics of ADP-dependent kinases including *Tl*GK have also shown the presence of a second conserved motif, known as HXE (i.e. His-Xaa-Glu, Fig. 1), whose glutamate is thought to participate in the second coordination sphere of the ADP-complexed magnesium cation and is located in proximity to the phosphoryl acceptor substrate [11]. The functional role of this residue still remains to be ascertained.

In this work we first employed site-directed mutagenesis and enzyme kinetics assays to evaluate the functional role of residues Glu279 and Glu308 from *Tl*GK, belonging to the HXE and NXXE motifs, respectively. Although mutations of the glutamate of both motifs had a large impact on the turnover rate of *Tl*GK, HXE mutants primarily affected the Michaelis constant (K_M) for glucose while NXXE mutants increased the K_M for $MgADP^-$. Moreover, increasing concentrations of free Mg^{2+} activated a mutant of Glu308 by Gln (E308Q) while, unexpectedly, replacements of Glu279 by Asp (E279D), Gln (E279Q) or Leu (E279L) did not change the inhibitory effect exerted by this divalent cation in the wild type enzyme. Then, we performed intrinsic fluorescence assays in the presence of a $MgADP^-$ analog, AMP–AlF_3, to assess whether glucose binding to the *Tl*GK·$MgADP^-$ was affected by the HXE mutations, showing a 87-fold increase in the dissociation constant (K_D) for glucose on the E279Q and E279L mutants, in comparison to the wild type enzyme and E308Q mutant. These results allow us to establish that the HXE motif is involved in the formation of the ternary complex required for the proper catalytic activity of *Tl*GK rather than in regulation of its activity by free divalent cations.

2. Material and methods

2.1. Expression and protein purification of TlGK

Wild type *Tl*GK and E279D, E279Q, E279L and E308Q mutants were overexpressed in *E. coli* strain BL21 (DE3) pLysS using the pET-17b expression vector. Cells were cultured at 37 °C in Luria Bertani broth medium containing 50 μg/ml of ampicillin and 35 μg/ml of chloramphenicol until $OD_{600} \sim 0.5$. Isopropyl-β-D-thiogalactopyranoside was then added to the medium to a final concentration of 1 mM to induce *Tl*GK overexpression, and cells were cultured overnight. Proteins were purified as described in Merino et al. [11], with some modifications. After incubating the crude extract at 90 °C for 30 min, the denatured proteins were removed by centrifugation (47 850*g* for 15 min). The supernatant was saturated with 60% $(NH_4)_2SO_4$ for 30 min and later centrifuged to remove protein precipitates. The soluble fraction was loaded onto a Phenyl Sepharose HP column (GE Healthcare, 5 ml) and then eluted with a linear gradient of $(NH_4)_2SO_4$ (from 60% to 0%). Active fractions were pooled, dialyzed against buffer A (Tris–HCl 50 mM, 5 mM $MgCl_2$, pH 7.8), subjected to anion exchange chromatography on a HiTrap Q HP column (GE Healthcare, 5 ml) and eluted using a lineal gradient of KCl (0–1 M). Active fractions were concentrated and used as the purified enzyme. The protein concentration was quantified using the Bradford assay [21].

2.2. Enzyme activity

Glucokinase activity was measured spectrophotometrically at 40 °C as previously described [7,11], coupling the formation of glucose-6-P to the reduction of NAD^+. The reaction mixture contained 50 mM HEPES pH 7.8, glucose, adenosine-diphosphate (ADP), and divalent metal, 0.5 mM NAD^+ and 1.4 units of glucose-6-P dehydrogenase from *Leuconostoc mesenteroides*. The change in NADH concentration was followed spectrophotometrically at 340 nm using an extinction coefficient of 6.22 $mM^{-1}\,cm^{-1}$ [22].

Kinetic parameters were determined by measuring the enzyme activities as a function of the concentration of glucose and $MgADP^-$ respectively, using saturating concentrations of the corresponding co-substrate, which were experimentally determined for each enzyme. The concentration of free Mg^{2+} was held constant at 1 mM for all the kinetic characterizations. Specific activities were calculated from initial velocities of NAD^+ reduction and expressed in units per mg of protein. The kinetic parameters were obtained by fitting the experimental curves to the Michaelis–Menten model [23], excepting the E308Q and E279D mutants for which the Haldane model for substrate inhibition was used [24]. Experimental data were fitted using GraphPad Prism 5.0 (GraphPad Software, Inc.).

2.3. Inhibition by free divalent cations

We evaluated the effect of increasing the concentration of free Mg^{2+} on the activity of wild type *Tl*GK and single-point mutants of residues Glu279 and Glu308, using saturating $MgADP^-$ and glucose concentrations for each enzyme. Concentrations between 0.75 mM and 10 mM of free Mg^{2+} were assayed. The results are shown as relative activity, taking the highest activity observed as 100% for each enzyme. The concentration of free Mg^{2+}, ADP^{3-} and $MgADP^-$ were calculated from the total concentration of ADP^{3-} and Mg^{2+} as in Merino et al. [11], using the equilibrium $MgADP^- \leftrightarrow ADP^{3-} + Mg^{2+}$. The dissociation constant (K_D) of this process (676 μM) was obtained from the Critical Metal Complexes Database Version 5.0 (Texas A&M University).

The effect of free metal on the catalytic turnover was assessed using a formalism previously proposed in Merino et al. [11], which considers that both the ternary complex formed by *Tl*GK and its substrates in the absence (ES) and presence (ESI) of a second cation are productive, as shown below:

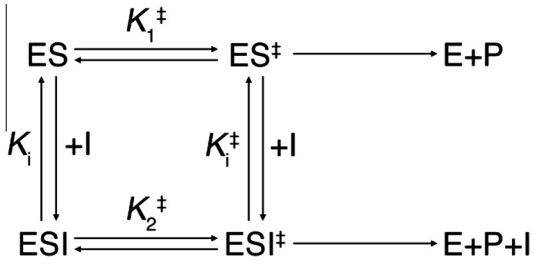

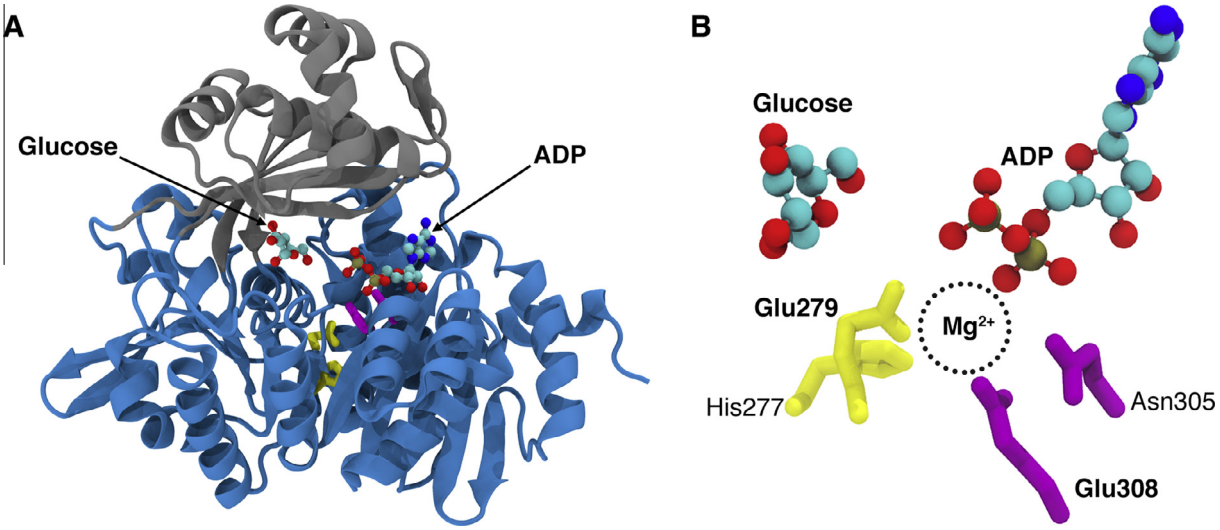

Fig. 1. Position of the NXXE and HXE motifs in the crystal structure of *Tl*GK. (A) Cartoon representation of the three-dimensional structure of *Tl*GK (PDB ID 4B8S), with its large domain in blue and its small domain in gray. The side chains of the conserved residues from HXE (yellow) and NXXE (purple) are shown as sticks, while ADP (PDB ID 1GC5) and glucose (4B8S) are shown in ball-and-stick representation and colored based on the atom types. (B) Position of the NXXE and HXE motifs around the donor and acceptor substrates. The representation of the side chains of the conserved residues from HXE (yellow) and NXXE (purple) and of the donor and acceptor substrates matches the scheme in (A). Also, the theoretical position of the magnesium cation that participates in the $MgADP^-$ complex is indicated.

where $ES^‡$ and $ESI^‡$ are the transition states of the ES and ESI complexes, $K_1^‡$ and $K_2^‡$ are the equilibrium constants between the ground and transition states for each complex, I is the inhibitor (here, free Mg^{2+}), P is the reaction product and K_i and $K_i^‡$ are the dissociation constants for the free Mg^{2+} cation and the ground state or transition state, respectively. A similar model was used to assess the effect of ligand binding in the unfolding rates of barnase [25]. In this model, the observed velocity is the combination of the production of both ES (ES → E + P) and ESI (ESI → E + P + I) as follows:

$$v = v_1 + v_2 = k_1[\mathrm{ES}] + k_2[\mathrm{ESI}] \quad (1)$$

Under the assumption of rapid equilibrium between ES and ESI, the observed velocity can be expressed as:

$$v = \left(\frac{k_1 K_i + k_2[\mathrm{I}]}{K_i + [\mathrm{I}]}\right)([\mathrm{ES}]_T) \quad (2)$$

where $[ES]_T = [ES] + [ESI]$. The estimated kinetic rates were related to the activation free energy through Eyring's formalism [26], as previously showed [11]. As noticeable from the thermodynamic cycle presented above, the difference between these activation free energies corresponds to the energetic contribution of the second Mg^{2+} ion to the stabilization of either the ground or transition state.

2.4. Fluorescence measurements of binding of glucose

The addition of glucose to *Tl*GK does not exert changes in the fluorescence intensity of any of its four Trp residues, unless a $MgADP^-$ analog is also present [10]. Therefore, assessment of glucose binding was carried out by measuring the change in fluorescence intensity upon titration of *Tl*GK in complex with the non-hydrolysable transition state analog of $MgADP^-$, AMP–AlF_3. AlF_3 is generally used to mimic the planar phosphoryl group in the catalytic transition state of many phosphatases and kinases [27–33]. Although it is generally used along with ADP, AlF_3 can also form complexes with AMP and other nucleotides and leads to inhibition of kinase activity [34], thus validating its use as an $MgADP^-$ analog.

For the fluorescence measurements, a reaction mixture containing HEPES 25 mM, AMP 10 mM, NaF 30 mM, $AlCl_3$ 1 mM and 5 μM of *Tl*GK was made. The excess of NaF over $AlCl_3$ used in the reaction mixture ensured that the concentration of AlF_3 formed was sufficient to inhibit the activity of the wild type enzyme (Fig. S6). The components were added separately, waiting 5 min for the stabilization of the fluorescence intensity. Then, the *Tl*GK·AMP–AlF_3 complex was titrated with increasing concentrations of glucose, ranging between 0 and 60 mM. The emission spectra were recorded in the range 300–500 nm upon excitation at 295 nm, with an excitation and emission slit of 3 nm. The increase of intrinsic fluorescence of *Tl*GK upon addition of glucose was recorded at 334 nm and the data were fitted to the model used in Yévenes et al. [35] for a protein–ligand equilibrium, considering that the change in intensity (Y_F) is proportional to the protein–ligand complex:

$$Y_F = \frac{\left|(E + L + K_D) - \sqrt{(E + L + K_D)^2 - 4EL}\right|}{2E} \quad (3)$$

where E is the concentration of *Tl*GK in the solution, L is the concentration of glucose added and K_D is the dissociation constant of the complex.

3. Results and discussion

3.1. HXE mutants impact on the catalytic turnover by affecting the K_M for glucose

Previous studies of the NXXE motif in other kinases have shown that mutations of its glutamate residue lead to lower turnover rate (k_{cat}) and higher K_M for $MgADP^-$ [12,17,20]. This is also true for the E308Q mutant of *Tl*GK, which has a 104-fold increase in K_M for the phosphoryl donor substrate and a 13-fold decrease in k_{cat} compared to the wild type protein, without significantly altering the K_M for glucose (Table 1 and Figs. S1 and S2). Analysis of the experimental data suggests that this mutant also experiences substrate inhibition, in contrast to wild type *Tl*GK (Fig. S1 and S2), although it is effective at very high concentrations of glucose (K_i = 860 ± 160 mM) and $MgADP^-$ (K_i = 70 ± 22 mM).

Since previous work suggested that the glutamate residue from the HXE motif was also participating in the coordination sphere of

the divalent cation from the metal–nucleotide complex [11], we expected that mutations of this residue would have a similar effect on the kinetic parameters as in the case of the E308Q mutant. As shown in Table 1, the k_{cat} values for all the HXE mutants are lower than wild type *Tl*GK and the E308Q mutant (Figs. S3–S5), ranging between a 38-fold (E279D) and a 103-fold (E279L) decrease when compared to the wild type enzyme. However, with the exception of E279D, these mutants marginally affect the K_M for $MgADP^-$. Notwithstanding, the reduced catalytic turnover of these mutants is accompanied by a large increase in K_M for glucose when compared to the wild type enzyme, being 29-fold higher for E279D, 32-fold higher for E279Q and 392-fold higher for E279L (Table 1). Also, the E279D mutant is inhibited by high concentrations of $MgADP^-$ (K_i = 24 ± 4 mM, Fig. S3).

These results suggest that the NXXE and HXE motifs play two non-overlapping roles in the enzymatic activity of *Tl*GK: the former participates in the stabilization of $MgADP^-$ in its binding site, while the latter participates in the interaction with glucose, suggesting an important role in catalysis and formation of the ternary complex. The next section addresses whether these motifs also participate in the inhibition exerted by free divalent cations on the activity of *Tl*GK.

3.2. HXE and NXXE mutants have dissimilar effects in enzyme activity regulation by free Mg^{2+}

Activation or inhibition by free divalent cations is a phenomenon that has been previously described in enzymes from the ribokinase superfamily and has been linked to the NXXE motif [12,15,20]. Recent studies on *Tl*GK have demonstrated that its activity is also strongly inhibited by increasing concentrations of free divalent cations [11], but the role of the HXE and NXXE motifs in this regulation has not been explored.

We performed kinetic assays of wild type *Tl*GK and HXE and NXXE mutants, where the concentration of free Mg^{2+} was increased from 0.75 mM to 10 mM while keeping $MgADP^-$ and glucose at the proper saturating concentrations for each enzyme. Our results show that the E308Q mutant of the NXXE motif is no longer inhibited by free Mg^{2+}, but rather activated (Fig 2 and Table 2). This is somewhat similar to the observations of the effect of NXXE mutants in the activity of human adenosine kinase, where the activation of the enzyme is shifted toward higher Mg^{2+} concentrations when compared to the wild type protein [12].

On the other hand, all of the HXE mutants show between 50% and 60% inhibition of glucokinase (GK) activity due to increasing concentrations of free Mg^{2+} (Fig. 2), similar to the behavior observed for the wild type enzyme. These results suggest that NXXE is the only highly conserved motif responsible for the Mg^{2+}-assisted regulation of the GK activity. By fitting the experimental data to Eq. (2), we were able to calculate the Mg^{2+} inhibition constant (K_i), and the activation constant (K_a) in the case of the E308Q mutant. As shown in Table 2, the K_i is very similar between the wild type protein and the HXE mutants, being on average 0.9 ± 0.2 mM, while the K_a for the E308Q mutant is 3.3 ± 0.2 mM.

Using Eyring's formalism [26] and the thermodynamic cycle that describes binding of a second cation to the ground and transition states of the reaction catalyzed by *Tl*GK (see Section 2), we calculated the free energy difference between both states upon binding of Mg^{2+}. As shown in Table 2, binding of the second cation leads to stabilization of the ground state for both the wild type enzyme and the HXE mutants, which explains the diminution of the reaction velocity for all these cases. Moreover, the rate of the reaction in the presence of a second cation (k_2) for all the HXE mutants is between 3 and 7 times slower than in its absence (k_1), while in the case of the wild type protein the ratio k_1/k_2 is ~2, which suggest that the HXE mutants also have a small effect in the rate of product formation in the presence of the second Mg^{2+} ion. In the case of the E308Q mutant, replacement of the glutamate residue leads to a slower rate in the absence of a second divalent cation (k_1) than in its presence (k_2) and an inversion of the sign of the change in free energy (Table 2), which explains why this mutant shows higher reaction velocities upon increasing concentrations of free Mg^{2+}, confirming previous suggestions by Merino et al. [11].

Finally, since mutations of the NXXE motif in *E. coli* phosphofructokinase-2 lead to changes in activation by Mg^{2+} and Mn^{2+} without prejudice of the ability to bind free divalent cations [17], and taking into account the sequential ordered substrate binding mechanism of *Tl*GK [7,10] along with the little to no impact of the HXE mutants in the K_M for $MgADP^-$, we argue that the NXXE motif is only related to the regulatory role exerted by free divalent cations in *Tl*GK, while the HXE motif is related to formation of the ternary complex required for the catalytic activity of this enzyme. We thus explored the formation of the ternary complex of *Tl*GK by intrinsic fluorescence, which is covered in the final section.

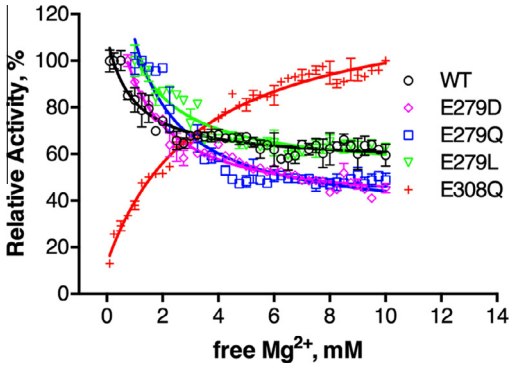

Fig. 2. Effect of free Mg^{2+} concentration on the activity of wild type *Tl*GK and mutants of the HXE and NXXE motifs. The activity of the wild type enzyme (black) and the E279D (pink), E279Q (blue), E279L (green) and E308Q (red) mutants were assayed at saturating $MgADP^-$ and glucose concentrations. The results are shown as relative activity, taking the highest measure activity as 100%. The lines represent the best fit to Eq. (2).

Table 1
Estimated kinetic parameters for wild type *Tl*GK and HXE and NXXE mutants.

Enzyme	V_{max} (U/mg)	k_{cat} (s^{-1})	K_M $MgADP^-$ (μM)	k_{cat}/K_M $MgADP^-$ (s^{-1} μM^{-1})	K_M glucose (μM)	k_{cat}/K_M glucose (s^{-1} μM^{-1})
Wild type[a]	69 ± 3	58 ± 3	14 ± 2	4.14	280 ± 15	2.07×10^{-1}
E279D[b]	5.68 ± 0.02	1.52 ± 0.02	270 ± 10	5.63×10^{-3}	8000 ± 600	1.9×10^{-4}
E279Q[a]	0.850 ± 0.003	0.710 ± 0.003	66 ± 1	1.07×10^{-2}	8900 ± 130	7.9×10^{-5}
E279L[a]	0.67 ± 0.01	0.56 ± 0.01	34 ± 3	1.64×10^{-2}	109700 ± 1500	5.1×10^{-6}
E308Q[b]	5.2 ± 0.2	4.3 ± 0.2	1460 ± 55	2.95×10^{-3}	390 ± 20	1.1×10^{-2}

All experiments were performed at a free Mg^{2+} concentration of 1 mM and constant temperature of 40 °C.
[a] Kinetic parameters determined by fitting the data to a Michaelis–Menten model.
[b] Kinetic parameters determined by fitting the data to a Haldane model of substrate inhibition.

Table 2
Estimated kinetic rates for the ternary complex in the absence and presence of a second cation, inhibition constant, activation constant and free energy difference between the ground and transition states due to binding of free Mg^{+2}.

Enzyme	k_1 (s^{-1})	k_2 (s^{-1})	K_i (mM)	K_a[a] (mM)	$\Delta\Delta G$[b] (kcal mol^{-1})
Wild-type	83 ± 2	42 ± 1	0.9 ± 0.2	–	−0.42 ± 0.01
E279D	1.72 ± 0.02	0.41 ± 0.01	0.9 ± 0.2	–	−0.89 ± 0.01
E279Q	2.5 ± 0.5	0.37 ± 0.03	0.8 ± 0.3	–	−1.2 ± 0.1
E279L	0.8 ± 0.1	0.23 ± 0.01	0.8 ± 0.3	–	−0.7 ± 0.1
E308Q	0.5 ± 0.1	4.7 ± 0.1	–	3.3 ± 0.2	1.4 ± 0.1

All parameters were determined from experiments using saturating concentrations of $MgADP^-$ and glucose at a constant temperature of 40 °C.
[a] Free Mg^{2+} behaves as an activator for E308Q, hence its activation constant (K_a) is reported.
[b] Free energy difference between the transition state and the ground state due to binding of the second Mg^{2+} as in Merino et al. [11].

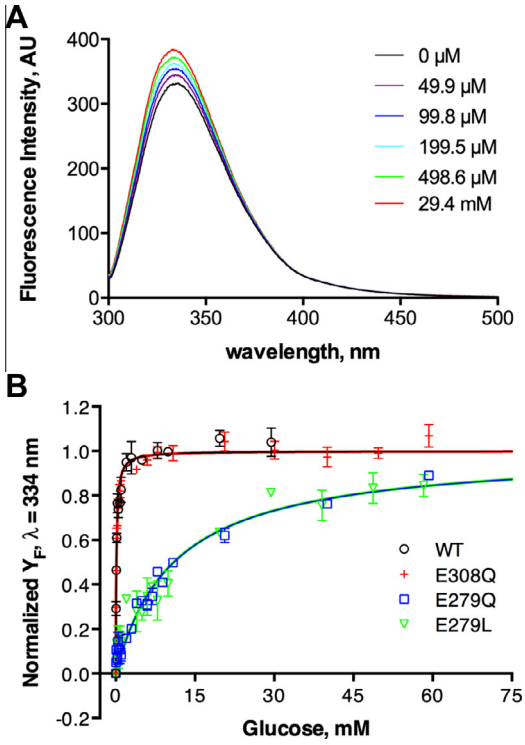

Fig. 3. Change in fluorescence intensity upon binding of glucose to the *Tl*GK·AMP–AlF_3 complex. (A) Increase in tryptophan fluorescence intensity upon addition of increasing concentrations of glucose onto the preincubated *Tl*GK·AMP–AlF_3 complex. The maximum of each spectrum is located at 334 nm. (B) Normalized fluorescence intensity change (Y_F) of wild type *Tl*GK (black) and E308Q (red), E279Q (blue) and E279L (green) mutants. The lines represent the best fit to Eq. (3).

3.3. HXE affects binding of glucose for the formation of the ternary complex

The large effect of replacing the glutamate residue of the HXE motif in the K_M for glucose, and the conservation of the inhibitory effect experienced by *Tl*GK upon binding of Mg^{2+}, favored the idea that this motif was related to binding of glucose onto the *Tl*GK·$MgADP^-$ complex, the second step in the sequential ordered substrate binding of this enzyme [7,10]. Since the individual addition of glucose does not lead to tryptophan fluorescence changes in *Tl*GK unless an $MgADP^-$ analog is present [10], we designed an experiment in which the enzyme forms a complex with a non-hydrolysable analog, AMP–AlF_3, where the aluminum fluoride is known to mimic the planar configuration of the phosphoryl group in the catalytic transition state of several nucleotides, including ADP and AMP [34].

Table 3
Estimated dissociation constant of glucose from the *Tl*GK·MgAMP–AlF_3 complex as measured by intrinsic fluorescence.

Enzyme	Wild-type	E308Q	E279Q	E279L
K_D (µM)	127 ± 12	130 ± 35	11 000 ± 1200	11 000 ± 2100

All the fluorescence experiments were performed at 40 °C.

The preincubation of *Tl*GK with AMP, $AlCl_3$ and NaF such that the concentration of AMP–AlF_3 formed is ~1 mM, followed by titration with increasing concentrations of glucose, led to a notorious increase in fluorescence intensity (Fig. 3A), in good agreement with previous assessment of glucose binding in the presence of MgAMP [10]. We fitted the change in fluorescence intensity of wild type *Tl*GK to Eq. (3) in order to estimate the dissociation constant for glucose (K_D), which was 127 ± 12 µM (Fig. 3B and Table 3), in excellent agreement with the K_M for glucose (Table 1). A similar K_D was estimated for the NXXE mutant E308Q, in line with the lack of significant changes on the K_M for glucose in this mutant.

In contrast, the HXE mutants E279Q and E279L showed a 87-fold increase in K_D for glucose (Fig. 3B and Table 3). While the K_D of the E279Q mutant is in good agreement with the corresponding K_M for glucose, the E279L mutant exhibits a much larger K_M for this substrate, which suggest that shortening and charge removal from the side chain of residue Glu279 also has a strong impact in the transfer of the phosphoryl group from $MgADP^-$ to the acceptor substrate. Altogether, these results provide strong evidence that the NXXE motif is related to regulation of the GK activity by free divalent cations and that the HXE motif participates in proper binding of glucose during formation of the ternary complex for catalysis.

4. Conclusions

Our results provide strong experimental evidence indicating that the highly conserved HXE motif is fundamental for glucose binding during the sequential ordered formation of the ternary complex required for the catalytic activity of *Tl*GK, rather than participating in the regulation of the enzyme by divalent cations, as in the case of the NXXE. While these results were unexpected, based on the preliminary evidence suggesting that the glutamate residue from the HXE and NXXE motifs were both part of the coordination sphere of magnesium from the $MgADP^-$ complex, they encourage the search for similar motifs in other members of the ribokinase superfamily and also for other residues that provide these enzymes with the ability to bind free divalent cations involved in regulation of their catalytic activity.

5. Conflict of interest

The authors declare no conflict of interest exists.

Acknowledgement

This work was supported by Fondo Nacional de Desarrollo Científico y Tecnológico (FONDECYT) Grants 1110137 & 1150460, Chile. We are grateful to Dr. Takayoshi Wakagi (University of Tokyo) from whom the expression vector containing glucokinase from *T. litoralis* was obtained.

The funders had no role in the study design, in the collection, analysis and interpretation of data, in the writing of the report or in the decision to submit the article for publication.

Appendix A. Supplementary data

Supplementary data associated with this article can be found, in the online version, at http://dx.doi.org/10.1016/j.febslet.2015.09.013.

References

[1] Verhees, C.H., Kengen, S.W.M., Tuininga, J.E., Schut, G.J., Adams, M.W.W., De Vos, W.M. and Van Der Oost, J. (2003) The unique features of glycolytic pathways in Archaea. Biochem. J. 375, 231–246.

[2] Ito, S., Fushinobu, S., Yoshioka, I., Koga, S., Matsuzawa, H. and Wakagi, T. (2001) Structural basis for the ADP-specificity of a novel glucokinase from a hyperthermophilic archaeon. Structure 9, 205–214.

[3] Rossmann, M.G., Moras, D. and Olsen, K.W. (1974) Chemical and biological evolution of nucleotide-binding protein. Nature 250, 194–199.

[4] Zhang, Y., Dougherty, M., Downs, D.M. and Ealick, S.E. (2004) Crystal structure of an aminoimidazole riboside kinase from *Salmonella enterica*: implications for the evolution of the ribokinase superfamily. Structure 12, 1809–1821.

[5] Mathews, I.I., Erion, M.D. and Ealick, S.E. (1998) Structure of human adenosine kinase at 1.5 Å resolution. Biochemistry 37, 15607–15620.

[6] Ramírez-Sarmiento, C.A., Baez, M., Zamora, R.A., Balasubramaniam, D., Babul, J., Komives, E.A. and Guixé, V. (2015) The folding unit of phosphofructokinase-2 as defined by the biophysical properties of a monomeric mutant. Biophys. J. 108, 2350–2361.

[7] Rivas-Pardo, J.A., Herrera-Morande, A., Castro-Fernandez, V., Fernandez, F.J., Vega, M.C. and Guixé, V. (2013) Crystal structure, SAXS and kinetic mechanism of hyperthermophilic ADP-dependent glucokinase from *Thermococcus litoralis* reveal a conserved mechanism for catalysis. PLoS One 8, e66687.

[8] Tsuge, H., Sakuraba, H., Kobe, T., Kujime, A., Katunuma, N. and Ohshima, T. (2002) Crystal structure of the ADP-dependent glucokinase from *Pyrococcus horikoshii* at 2.0-A resolution: a large conformational change in ADP-dependent glucokinase. Protein Sci. 11, 2456–2463.

[9] Ito, S., Fushinobu, S., Jeong, J.J., Yoshioka, I., Koga, S., Shoun, H. and Wakagi, T. (2003) Crystal structure of an ADP-dependent glucokinase from *Pyrococcus furiosus*: implications for a sugar-induced conformational change in ADP-dependent kinase. J. Mol. Biol. 331, 871–883.

[10] Rivas-Pardo, J.A., Alegre-Cebollada, J., Ramírez-Sarmiento, C.A., Fernandez, J.M. and Guixé, V. (2015) Identifying sequential substrate binding at the single-molecule level by enzyme mechanical stabilization. ACS Nano 9, 3996–4005.

[11] Merino, F., Rivas-Pardo, J.A., Caniuguir, A., García, I. and Guixé, V. (2012) Catalytic and regulatory roles of divalent metal cations on the phosphoryl-transfer mechanism of ADP-dependent sugar kinases from hyperthermophilic archaea. Biochimie 94, 516–524.

[12] Maj, M.C., Singh, B. and Gupta, R.S. (2002) Pentavalent ions dependency is a conserved property of adenosine kinase from diverse sources: identification of a novel motif implicated in phosphate and magnesium ion binding and substrate inhibition. Biochemistry 41, 4059–4069.

[13] Musayev, F.N., di Salvo, M.L., Ko, T.-P., Gandhi, A.K., Goswami, A., Schirch, V. and Safo, M.K. (2007) Crystal structure of human pyridoxal kinase: structural basis of M(+) and M(2+) activation. Protein Sci. 16, 2184–2194.

[14] Navarro, F., Ramírez-Sarmiento, C.A. and Guixé, V. (2013) Catalytic and regulatory roles of species involved in metal–nucleotide equilibriums in human pyridoxal kinase. Biometals 26, 805–812.

[15] Parducci, R.E., Cabrera, R., Baez, M. and Guixé, V. (2006) Evidence for a catalytic Mg^{2+} ion and effect of phosphate on the activity of *Escherichia coli* phosphofructokinase-2: regulatory properties of a ribokinase family member. Biochemistry 45, 9291–9299.

[16] Cabrera, R., Ambrosio, A.L.B., Garratt, R.C., Guixé, V. and Babul, J. (2008) Crystallographic structure of phosphofructokinase-2 from *Escherichia coli* in complex with two ATP Molecules. Implications for substrate inhibition. J. Mol. Biol. 383, 588–602.

[17] Rivas-Pardo, J.A., Caniuguir, A., Wilson, C.A.M., Babul, J. and Guixé, V. (2011) Divalent metal cation requirements of phosphofructokinase-2 from *E. coli*. Evidence for a high affinity binding site for Mn^{2+}. Arch. Biochem. Biophys. 505, 60–66.

[18] Li, M.H., Kwok, F., Chang, W.R., Lau, C.K., Zhang, J.P., Lo, S.C.L., Jiang, T. and Liang, D.C. (2002) Crystal structure of brain pyridoxal kinase, a novel member of the ribokinase superfamily. J. Biol. Chem. 277, 46385–46390.

[19] Miallau, L., Hunter, W.N., McSweeney, S.M. and Leonard, G.A. (2007) Structures of *Staphylococcus aureus* D-tagatose-6-phosphate kinase implicate domain motions in specificity and mechanism. J. Biol. Chem. 282, 19948–19957.

[20] Quiroga-Roger, D., Babul, J. and Guixé, V. (2015) Role of monovalent and divalent metal cations in human ribokinase catalysis and regulation. Biometals 28, 401–413.

[21] Bradford, M.M. (1976) A rapid and sensitive method for the quantitation of microgram quantities of protein using the principle of protein dye binding. Anal. Biochem. 72, 248–254.

[22] Kornberg, A. and Pricer, W.E. (1953) Enzymatic esterification of alpha-glycerophosphate by long chain fatty acids. J. Biol. Chem. 204, 345–357.

[23] Michaelis, L. and Menten, M.L. (1913) Die Kinetik der Invertinwirkung. Biochemistry, 333–369.

[24] Briggs, G.E. and Haldane, J.B.S. (1925) A note on the kinetics of enzyme action. Biochem. J. 19, 338–339.

[25] Sancho, J., Meiering, E.M. and Fersht, A.R. (1991) Mapping transition states of protein unfolding by protein engineering of ligand-binding sites. J. Mol. Biol. 221, 1007–1014.

[26] Eyring, H. (1935) The activated complex in chemical reactions. J. Chem. Phys. 3, 107–115.

[27] Lunardi, J., Dupuis, A., Garin, J., Issartel, J.P., Michel, L., Chabre, M. and Vignais, P.V. (1988) Inhibition of H+-transporting ATPase by formation of a tight nucleoside diphosphate-fluoroaluminate complex at the catalytic site. Proc. Natl. Acad. Sci. U.S.A. 85, 8958–8962.

[28] Schlichting, I. and Reinstein, J. (1997) Structures of active conformations of UMP kinase from *Dictyostelium discoideum* suggest phosphoryl transfer is associative. Biochemistry 36, 9290–9296.

[29] Nadanaciva, S., Weber, J. and Senior, A.E. (1999) Binding of the transition state analog MgADP-fluoroaluminate to F1-ATPase. J. Biol. Chem. 274, 7052–7058.

[30] Braig, K., Menz, R.I., Montgomery, M.G., Leslie, A.G. and Walker, J.E. (2000) Structure of bovine mitochondrial F1-ATPase inhibited by Mg^{2+} ADP and aluminium fluoride. Structure 8, 567–573.

[31] Zhou, T., Radaev, S., Rosen, B.P. and Gatti, D.L. (2001) Conformational changes in four regions of the *Escherichia coli* ArsA ATPase link ATP hydrolysis to ion translocation. J. Biol. Chem. 276, 30414–30422.

[32] Madhusudan, Akamine P., Xuong, N.-H. and Taylor, S.S. (2002) Crystal structure of a transition state mimic of the catalytic subunit of cAMP-dependent protein kinase. Nat. Struct. Biol. 9, 273–277.

[33] Stamos, J.L., Chu, M.L.H., Enos, M.D., Shah, N. and Weis, W.I. (2014) Structural basis of GSK-3 inhibition by N-terminal phosphorylation and by the Wnt receptor LRP6. Elife.

[34] Miles, R.D., Gorrell, A. and Ferry, J.G. (2002) Evidence for a transition state analog, MgADP-aluminum fluoride-acetate, in acetate kinase from *Methanosarcina thermophila*. J. Biol. Chem. 277, 22547–22552.

[35] Yévenes, A., Espinoza, R., Rivas-Pardo, J.A., Villarreal, J.M., González-Nilo, F.D. and Cardemil, E. (2006) Site-directed mutagenesis study of the microenvironment characteristics of Lys213 of *Saccharomyces cerevisiae* phosphoenolpyruvate carboxykinase. Biochimie 88, 663–672.